Available online at www.sciencedirect.com
SCIENCE DIRECT
Journal of Molecular Catalysis A: Chemical 247 (2006) 283–290
JOURNAL OF MOLECULAR CATALYSIS A: CHEMICAL
www.elsevier.com/locate/molcata

Photocatalytic degradation of methylene blue on Bi_2MNbO_7 (M = Al, Fe, In, Sm) sol–gel catalysts

Lorena L. Garza-Tovar [a], Leticia M. Torres-Martínez [a,*], D. Bernal Rodríguez [a], R. Gómez [b], G. del Angel [b]

[a] *Departamento de Ecomateriales y Energía, Facultad de Ingeniería Civil, Universidad Autónoma de Nuevo León, Ciudad Universitaria, Apartado Postal 17, San Nicolás de los Garza, Nuevo León 66450, Mexico*
[b] *Departamento de Química, Universidad Autónoma Metropolitana-1ztapalapa, Area de Catálisis, Av. San Rafael Atlixco No. 186, Apartado Postal 55-534, México D.F. 09340, Mexico*

Received 22 October 2005; received in revised form 25 November 2005; accepted 28 November 2005
Available online 10 January 2006

Abstract

Photocatalysts with general formula Bi_2MNbO_7 (M = In, Al, Fe, Sm) have been prepared following the sol–gel method by gelling niobium ethoxide with bismuth acetate and In, Al, Fe and Sm precursors. XRD, TGA/DTA, FT-IR, UV–vis, SEM and nitrogen adsorption techniques were used to characterize the solids. The evolution of the crystalline phases of the sol–gel samples with the annealing temperature was followed by XRD. At annealing temperatures lower than 400 °C crystalline Bi_2MNbO_7 phases were not detected, while at 800 °C only pyrochlore phase was observed. The energy band gap values were found from the UV–vis spectra of the samples calcined at 400 °C between 1.43 and 2.24 eV. Kinetic $t_{1/2}$ (half life) parameters for the photodegradation of methylene blue shown that Bi_2FeNbO_7 sol–gel catalysts were more active ($t_{1/2}$ = 13 min) than TiO_2 P-25 ($t_{1/2}$ = 45 min) reference photocatalyst. For comparative purposes solid state preparations of Bi_2MNbO_7 were also studied, showing a lower photocatalytic activity than the sol–gel preparations but it was in the same order of TiO_2 P-25 catalyst.

Keywords: Photocatalytic oxidation; Ceramic semiconductors; Pyrochlore structures; Sol–gel photocatalysts; Dyes photodegradation

1. Introduction

Heterogeneous photocatalytic processes for wastewater treatment have been recently used for the degradation of organic compounds to carbon dioxide, water and mineral ions with successful results [1–3]. For example, azo-dyes like alizarin S, crocein orange G, methyl red, congo red and methylene blue have been completely mineralized with TiO_2/UV in aqueous suspensions [4,5]. Nowadays, the most used photocatalyst is commercially available TiO_2, but its efficiency depends on the UV source [6,7]. The search for new promising photocatalysts that operate with visible light is an important challenge to extend the range of their applications [8–10]. In this way, recent papers report a new series of ceramic photocatalysts Bi_2MNbO_7 (M = Al^{3+}, Ga^{3+}, In^{3+} Fe^{3+}, Sm^{3+}, La^{3+}, Pr^{3+}), synthesized by solid state reaction. They have the pyrochlore structure $A_2{}^{3+}B_2{}^{4+}O_7$ and have shown photocatalytic activity for water splitting [11–13]. It is well known that the photocatalytic activity depends on the preparation method [14] finding desirable the production of powders with high specific surface area. Photoactive ceramic compounds can be produced by solid state reactions but their photocatalytic activities are limited because of their low specific surface area. Solids with the same chemical composition, similar structure and high specific surface area can be prepared by the sol–gel method under soft reaction conditions. With this in mind, in the present work we prepare Bi_2MNbO_7 (M = In, Al, Fe, Sm) by both the sol–gel method and solid state reaction. The comparison of activities was made on the photocatalytic degradation of methylene blue.

* Corresponding autor at: Universidad Autónoma de Nuevo León, Facultad de Ingeniería Civil, Av. Universidad y Av. Fidel Velazquez S/N Cd. Universitaria, San Nicolás de los Garza, Nuevo León 66450, Mexico.
Tel.: +52 81 8332 1902x112/8376 3979; fax: +52 81 8376 0477/8332 1902.
E-mail address: ltorres@ccr.dsi.uanl.mx (L.M. Torres-Martínez).

1381-1169/$ – see front matter © 2005 Elsevier B.V. All rights reserved.
doi:10.1016/j.molcata.2005.11.053

2. Experimental section

2.1. Sample preparation

2.1.1. Sol–gel synthesis

The Bi_2MNbO_7 (M = Al, In, Fe, Sm) compounds were prepared using stoichiometric amounts of aluminum isopropoxide (Aldrich 99.9%), indium isopropoxide (Aldrich 99.9%), iron acetylacetonate (Aldrich 99.9%) or samarium acetate (Aldrich 99.9%). They were dissolved in a 250 mL flask containing 100 mL of a solution ethanol/water 3:2. Then, pH was adjusted to 3 with nitric acid and the solution was refluxed for 3 h. Next, the respectively stoichiometric amounts of bismuth acetate (Aldrich 99.9%) in ethanol/water 1:1 solution and niobium ethoxide (Aldrich 99.9%) in ethanol were added drop by drop. Afterwards, pH was again adjusted to 9 and the solution was maintained under reflux until gelation, 5–10 days depending on the synthesized compound.

Samples were cured for 24 h and then the solvent was evaporated at 70 °C. The samples were dried in an oven at 70 °C in order to obtain fresh gels. Finally, they were annealed in air at 200, 400, 600 and 800 °C for 6 h.

2.1.2. Solid state reaction

Stoichiometric amounts of Bi_2O_3, Nb_2O_5, Al_2O_3, In_2O_3, Fe_2O_3, and Sm_2O_3 were mixed, pressed into pellets and heated slowly from room temperature to 900 °C for a few hours. Isothermal treatments in air were given at 900–1100 °C for 1–96 h depending on the composition, with intermediate regrinding to complete reaction.

2.2. Characterization

2.2.1. X-ray diffraction

The resulting samples were analyzed by X-ray powder diffraction with a D-5000 SIEMENS diffractometer, using Cu $K\alpha_1$ radiation.

2.2.2. Thermogravimetric analysis

TGA/DTA was used to determine the thermal evolution of the fresh gels using a SDT-2960, TA-Instruments in nitrogen flow.

2.2.3. FT-IR analysis

The infrared spectra were recorded with a Paragon 1000, Perkin-Elmer spectrophotometer in the wavenumber range of 4000–400 cm^{-1}.

2.2.4. UV–vis spectroscopy

Diffuse reflectance spectra of the samples were obtained in the 900–300 nm range, using a Lambda 12, Perkin-Elmer spectrophotometer equipped with an integration sphere RSA-PE-20. A standard USRS-99010, of Spectralon was used as 100% reflectance reference.

2.2.5. Scanning electron microscopy

Morphological microanalysis was performed using a S440, Leica microscope using secondary and backscattered electrons.

2.3. Photocatalytic evaluation

The light source used in the photodegradation experiments was a UV lamp Black-Ray XX-15L, with a wavelength of 254 nm and intensity of 1600 $\mu W/cm^2$. The lamp was set at a distance of 15 cm above a glass vessel of 250 mL containing 200 mL of aqueous solution, 30 ppm of methylene blue and 1 mL of H_2O_2 (30 vol.%). Before the photocatalytic experiments were carried out, the suspension was maintained under stirring for 60 min in the dark to establish the reactant adsorption equilibrium. The intensity of the light in the reactor vessel was 1100 $\mu W/cm^2$, determined with a UVX-25 UVP radiometer equipped with a 254 nm sensor. One hundred milligrams of catalyst were added in each experiment. Aliquots of the solution were taken at intervals of 15 min for 2.5 h. The concentration of methylene blue was calculated in function of time by measuring the 664 nm methylene blue absorption band with the UV–vis spectrophotometer.

3. Results and discussion

3.1. X-ray diffraction

The crystalline phases formed during the thermal treatment of the Bi_2MNbO_7 (M = Al^{3+}, In^{3+}, Fe^{3+}, Sm^{3+}) compounds were determined by XRD. In Fig. 1, the XRD patterns of Bi_2FeNbO_7 calcined at different temperatures are shown. In annealed samples at 200 and 400 °C some diffraction peaks can be observed.

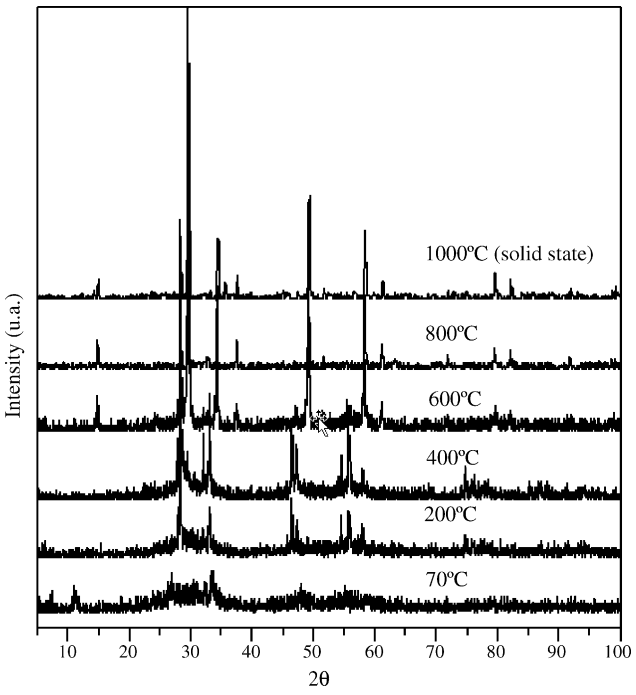

Fig. 1. X-ray powder pattern of Bi_2FeNbO_7 prepared by sol–gel at different temperatures.

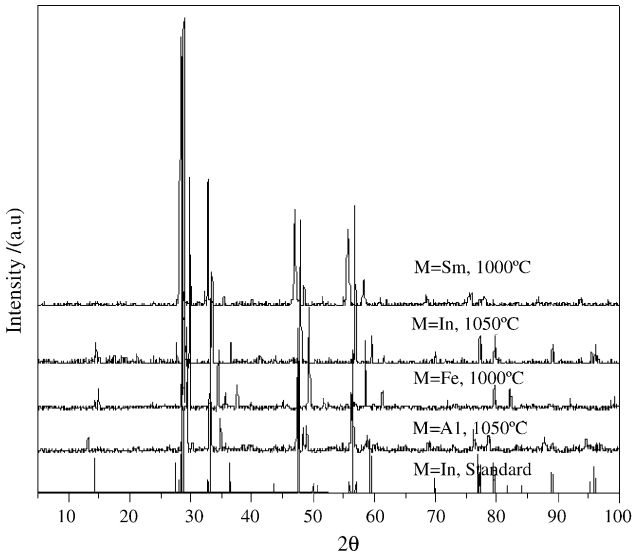

Fig. 2. X-ray powder pattern of Bi_2MNbO_7 ($M = Al^{3+}$, In^{3+}, Fe^{3+}, Sm^{3+}) synthesized by solid state reaction.

These peaks correspond to small amounts of unreacted Fe_2O_3 [15] and to the binary phase $Bi_5Nb_3O_{15}$ [16]. The presence of the Bi_2FeNbO_7 phase and small amount of $Bi_5Nb_3O_{15}$ are observed in the annealed sample at 600 °C. The sample calcined at 800 °C, showed the higher crystallinity in which case the Bi_2FeNbO_7, is the only phase observed.

The other Bi_2MNbO_7 ($M = Al^{3+}$, In^{3+}, Sm^{3+}) compounds show amorphous structure at temperatures lower than 400 °C. In these samples, the formation of trivalent oxides is not observed. At higher temperatures 600–800 °C the XRD pattern shows only the formation of the Bi_2MNbO_7 single phase.

X-ray diffraction patterns corresponding to solid state preparations of Bi_2MNbO_7 samples are shown in Fig. 2. Solid state preparations showed standard patterns corresponding to Bi_2InNbO_7 ceramic compound as calculated from the cell parameters and atomic positions reported by Zou et al. [17]. For the Bi_2AlNbO_7 and Bi_2SmNbO_7 ceramic compounds, the corresponding diffraction peaks are shifted to the left, meaning that the cell parameters are increasing which agree with the higher ionic ratios. Diffraction peaks for Bi_2FeNbO_7 are shifted to the right; attributed to the smaller ionic ratio of the trivalent metal. It is important to mention that we found different thermodynamic synthesis conditions than those previously reported by Zou et al. [17], since we found lower temperatures (1000–1050 °C) of reaction. Notice that the XRD patterns of all Bi_2MNbO_7 sol–gel samples annealed at 800 °C shown the same reflection peaks than the corresponding solid state preparations.

3.2. Thermal analysis

The evolution of fresh Bi_2FeNbO_7 sol–gel sample was followed by TGA/DTA (Fig. 3). The TGA shows four weight loss steps. The first one (I) appears between 30 and 150 °C (2.5 wt.%) corresponding to water desorption. The second weight loss (II) occurs in the range of 150–240 °C (12 wt.%), attributed to coordinated water desorption. DTA curve shows three thermal

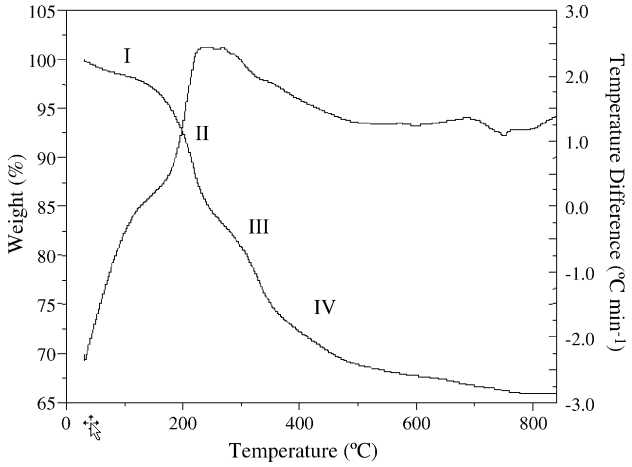

Fig. 3. DTA and TGA plots of Bi_2FeNbO_7 prepared by sol–gel.

events. The first broad exothermic peak observed in the range 25–250 °C corresponds to two thermal events, the weight loss of water and to the beginning of the crystallization of $Bi_5Nb_3O_{15}$, in agreement with the results observed by XRD. The third weight loss (III) appears in the temperature range of 250–350 °C (10 wt.%), associated to the decomposition of residual alkoxy groups. A slight endothermic change on the slope of DTA curve occurs between 250 and 350 °C associated to third TGA step. The last weight loss (IV) (5 wt.%) was observed in the temperature range of 370–450 °C. This step corresponds to the complete dehydroxylation of the sample [18]. In the temperature range of 400–600 °C an exothermic event occurred which, we associate it to a structural transition, corresponding to the formation of the ternary phase as showed by XRD (Fig. 1).

3.3. Infrared spectroscopy

The infrared spectra of the sol–gel Bi_2AlNbO_7 sample treated at various temperatures are shown in Fig. 4. For the fresh sam-

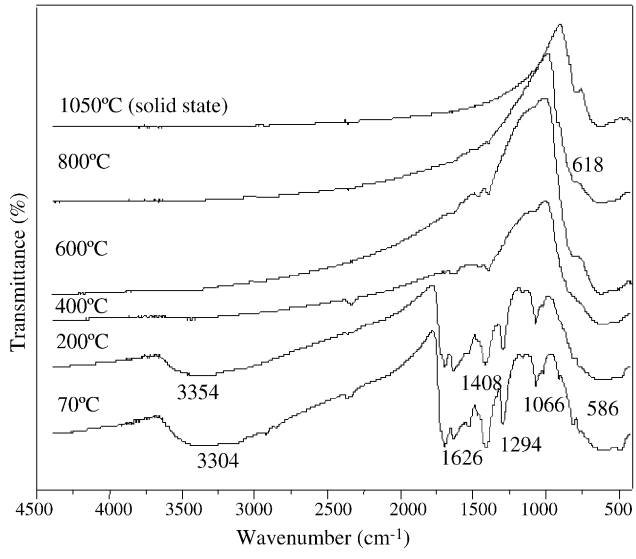

Fig. 4. Infrared spectra of thermal evolution of $Bi_2AlNbO7$ sol–gel.

ple dried at 70 °C, we can observe a broad absorption band at 3304 cm^{-1} assigned to H-bridges or either hydroxyl groups or water molecules bonded on the oxide surface trough H-bonding [18]. The intensity of this band decreases as the annealing temperature increases, since water is gradually desorbed. When the sample was annealed at 400–800 °C in the 3300–3400 cm^{-1} region no peaks are observed. At this temperature range the formation of the Bi_2AlNbO_7 took place according to the XRD results.

In the 1690–500 cm^{-1} region, we can observe an adsorption band at 1626 cm^{-1} assigned to the bending OH– vibrations of residual surface hydroxylic groups, at 70 and 200 °C, however, it disappeared at 400 °C, due to complete dehydroxylation. The adsorption band observed at 1408 cm^{-1} is related to symmetric and asymmetric C–H bending vibrations of CH_2 and CH_3 groups. This band decreases with thermal treatment due to desorption of residual solvents [18,19]. The band observed at 1294 cm^{-1} in the spectra of the fresh sample corresponds to the stretching vibration of C–OH bonds [20]. This band decreases in intensity until it became as a small shoulder when the sample was annealed at 400 °C.

Characteristic vibration bands of M–O bonds are observed in the low energy region of the spectra [19]. In sol–gel samples this band is observed between 618 and 586 cm^{-1} and increases in intensity as the annealing temperature increases. For solid state prepared materials this band appeared between 600 and 480 cm^{-1}. FT-IR spectra are in agreement with DTA/TGA and XRD patterns.

3.4. UV–vis spectroscopy

The energy band gap (E_g) values for the different samples annealed at 400 °C were calculated using the equation $\alpha(h\nu) = A(h\nu - E_g)^{m/2}$, where α is the absorption coefficient, $h\nu$ is the photon energy, A is a constant and $m = 1$ represents a direct transition between valence band and conduction band. For the estimation of E_g from the UV–vis spectra, a straight line was extrapolated from the absorption curve to the abscissa axis. When α has a value of 0, then $E_g = h\nu$.

UV–vis diffuse reflectance spectra of the sol–gel selected sample Bi_2AlNbO_7 are shown in Fig. 5, where two slopes at 400 °C and only one at 600 and 800 °C can be seen. The lower E_g values for the two slopes were obtained in the sample $Bi_2FeNbO7$ (1.43 and 1.71 eV) and the higher ones in the Bi_2AlNbO_7 sample (2.24 and 2.65 eV). These results agree well with the XRD analysis that shows the presence of two phases at 400 °C (Bi_2MNbO_7 and $Bi_5Nb_3O_{15}$) and the compound Bi_2MNbO_7, as a single phase at 800 °C. The E_g values for the different sol–gel catalysts are reported in Table 1, where the E_g value for TiO_2 P-25 reference photocatalyst is also included.

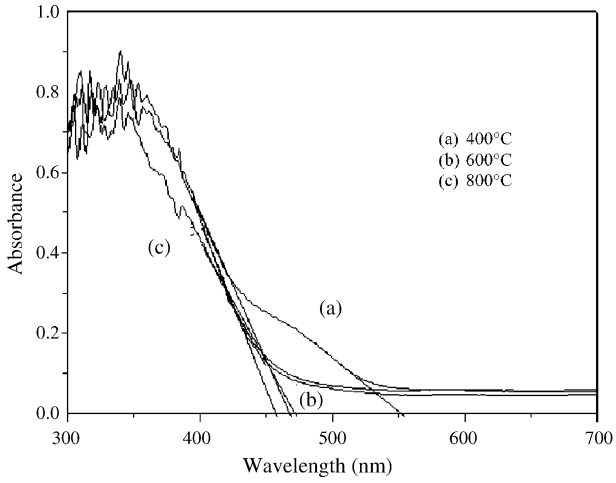

Fig. 5. UV–vis spectra of Bi_2AlNbO_7 sol–gel heated at different temperatures.

The effect of annealing temperature in the E_g was studied in the Bi_2FeNbO_7 sample annealed at 400, 600 and 800 °C, and the obtained values are reported in Table 2. They show that the E_g increases with the annealing treatment. It must be noted that in all of the cases, the energy band gap values were lower than those obtained in TiO_2 P-25 reference catalyst. Furthermore, solid state prepared materials present E_g values comprised between 1.84 and 2.63 eV (Table 3) lower than that of TiO_2 (3.2 eV).

Table 2
Characterization and photocatalytic activity on the methylene blue degradation of Bi_2FeNbO_7 sol–gel prepared materials calcined at different temperatures

Catalyst	T (°C)	BET area (m^2/g)	E_g (eV)	$t_{1/2}$ (min)
Bi_2FeNbO_7	400	20	1.43, 1.71	13
	600	5	1.9	32
	800	<1	1.75	47

Table 3
Energy band gap and photocatalytic activity on the methylene blue degradation of Bi_2MNbO_7 (M = Al^{3+}, In^{3+}, Fe^{3+}, Sm^{3+}) solid state prepared materials (1050 °C)

Catalyst	E_g (eV)	$t_{1/2}$ (min)	Catalyst	E_g (eV)	$t_{1/2}$ (min)
Bi_2AlNbO_7	2.63	30	Bi_2FeNbO_7	1.84	37
Bi_2InNbO_7	2.62	37	Bi_2SmNbO_7	2.48	37

Table 1
Characterization and photocatalytic activity on the methylene blue degradation of Bi_2MNbO_7 (M = Al^{3+}, In^{3+}, Fe^{3+}, Sm^{3+}) sol–gel prepared materials calcined at 400 °C

Catalyst	BET area (m^2/g)	E_g (eV)	$t_{1/2}$ (min)	Catalyst	BET area (m^2/g)	E_g (eV)	$t_{1/2}$ (min)
Bi_2AlNbO_7	22	2.24, 2.65	18	Bi_2FeNbO_7	20	1.43, 1.71	13
Bi_2InNbO_7	23	1.62, 2.20	27	Bi_2SmNbO_7	21	2.23, 2.57	18

TiO_2 P-25; BET area = 51 m^2/g; E_g = 3.20 eV; $t_{1/2}$ = 45 min.

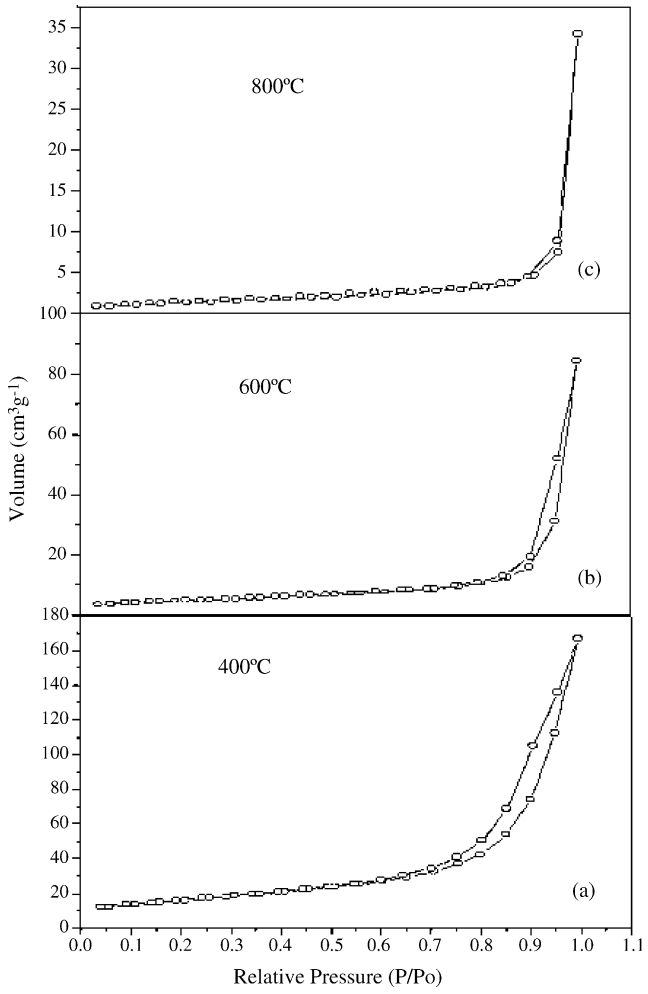

Fig. 6. Nitrogen adsorption isotherms for Bi_2AlNbO_7 sol–gel heated at different temperatures.

3.5. Textural properties

The specific surface areas were estimated from the nitrogen adsorption–desorption isotherms using the BET method. As an example, Fig. 6 shows the nitrogen adsorption–desorption isotherms for the Bi_2AlNbO_7 sol–gel compound, annealed at various temperatures. For the sample treated at 400 °C, a specific surface area of 22 m^2/g is obtained, while for samples treated at 600 and 800 °C, the specific surface area strongly diminishes, giving values of 7 and 2 m^2/g, respectively. In all the sol–gel samples similar behavior is observed, the specific surface areas go down with thermal treatments. The calculated specific surface areas for the Bi_2MNbO_7 sol–gel samples annealed at 400 °C are reported in Table 1. The effect of thermal treatment in Bi_2FeNbO_7 samples can be seen in Table 2.

The specific surface areas obtained in solid state ceramic compounds are lower than 1 m^2/g. These values are of the same order to those obtained in Bi_2FeNbO_7 sol–gel sample calcined at 800 °C (<1 m^2/g).

3.6. Scanning electron microscopy

SEM micrographs in the backscattered electrons mode for the Bi_2AlNbO_7 compound thermally treated at different temperatures are shown in Fig. 7. For the sample annealed at 200 °C, very small grain size particles can be seen forming clusters of not well defined form (Fig. 7(a)). The micrograph in Fig. 7(b) corresponds to the sample calcined at 400 °C, where very fine particles forming clusters are also observed. We can see small grains and the formation of needles, which is evidence of the presence of two phases (ternary Bi_2AlNbO_7 and binary $Bi_5Nb_3O_{15}$) as have been observed by XRD and suggested from the UV–vis spectroscopic analysis.

Fig. 7(c) and (d) correspond to samples treated at 600 and 800 °C, respectively. Similar clusters of fine particles are observed with grain sizes of about 0.5 μm. However, needles are not observed, indicating that only the single phase Bi_2AlNbO_7 is present at this temperature. Similar behavior was observed in all Bi_2MNbO_7 sol–gel samples.

For comparison, Fig. 7(e) and (f) show the electron micrograph of Bi_2MNbO_7 ($M = Al^{3+}$, In^{3+}) phase obtained by solid state method. These samples showed a high degree of sintering and most of the grains present flat surfaces. Average grain size for both materials is about 30–40 μm.

3.7. Photocatalytic evaluation

We found that the photocatalytic degradation of methylene blue follows a kinetic of pseudo-first order and the activity was expressed at the time to obtain 50% conversion (half time life, $t_{1/2}$). Since the specific surface areas of sol–gel samples strongly diminish with annealing temperature, we chose for methylene blue photocatalytic degradation the samples treated at 400 °C since all of them have similar BET areas around 20 m^2/g.

The degradation of methylene blue as a function of time for the Bi_2MNbO_7 sol–gel samples (400 °C) is shown in Fig. 8. We carried out also the photocatalytic reaction using TiO_2 (Degussa P25) as reference material.

Plots on Fig. 9 show that the photocatalytic activity for Bi_2MNbO_7 sol–gel samples is higher than that of TiO_2. It can also be observed that the sol–gel Bi_2FeNbO_7 sample presents the higher photocatalytic activity ($t_{1/2}$ = 13 min) for methylene blue photodegradation. On the other hand, for Bi_2AlNbO_7, Bi_2SmNbO_7 and Bi_2InNbO_7 catalysts, $t_{1/2}$ values were 18, 18 and 27 min, respectively. In Table 1, the $t_{1/2}$ values obtained from Fig. 9 are reported. Photocatalytic activity depends on many factors, among them, the E_g and the specific surface area of the photocatalysts. In our case, we can observe in Table 1 that the specific surface area of the samples annealed at 400 °C, is of the same order (20 m^2/g) and then this parameter can be pointed out as an important factor to explain the behavior of the sol–gel samples. In Table 1, it can be seen that the photoactivity for the different samples increases as the E_g value diminishes. We can then associate the lower E_g values as an important factor in catalytic activity efficiency.

The high efficiency presented by Bi_2FeNbO_7 (sol–gel at 400 °C) could also be attributed to Fe_2O_3 observed by XRD

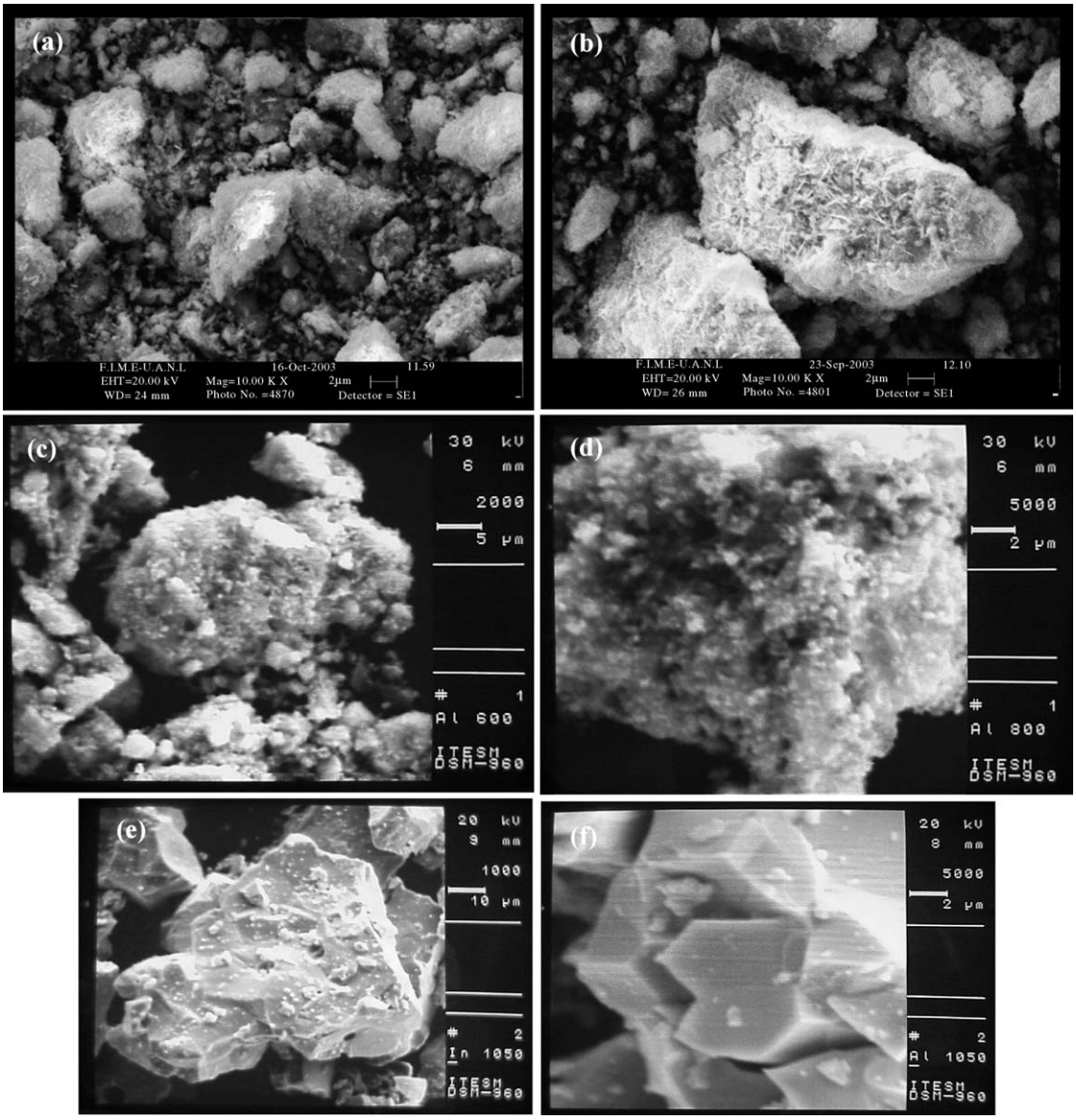

Fig. 7. Micrographs of sol–gel Bi_2AlNbO_7 (200, 400, 600 and 800 °C) and solid state Bi_2AlNbO_7 ($M = Al^{3+}$ and In^{3+}) materials.

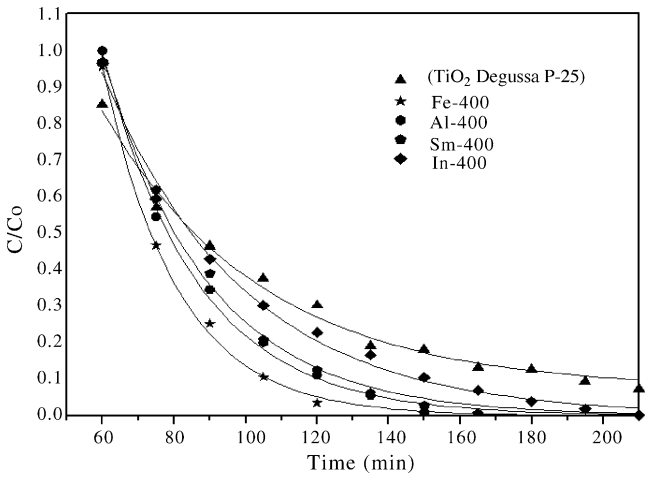

Fig. 8. Photodecomposition as a function of time of methylene blue on Bi_2MNbO_7 ($M = Al^{3+}$, In^{3+}, Fe^{3+}, Sm^{3+}) sol–gel.

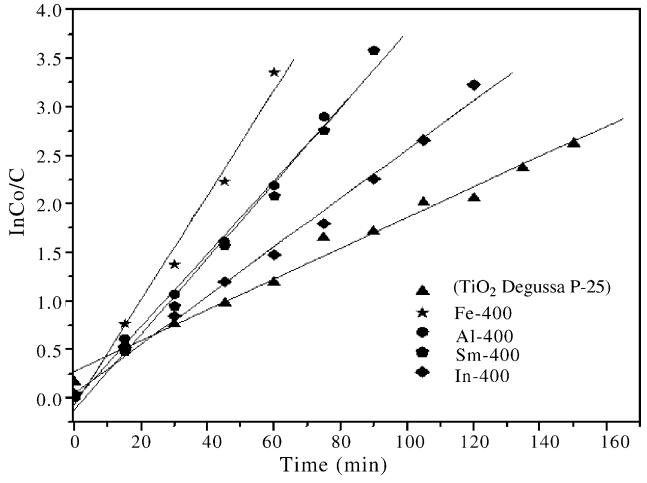

Fig. 9. Plots for kinetic parameters determination in methylene blue degradation by sol–gel compounds.

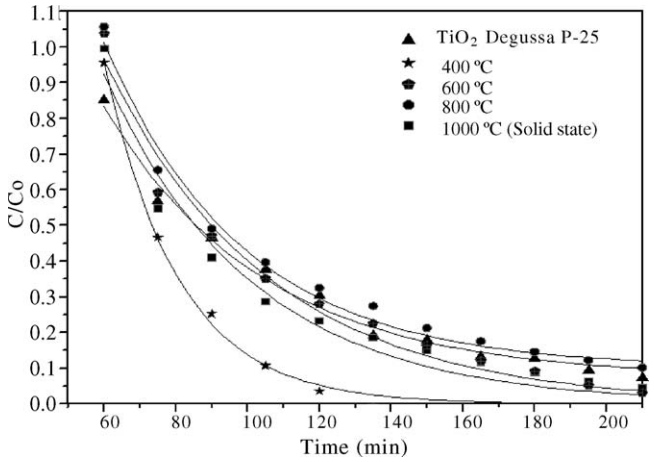

Fig. 10. Photodecomposition as a function of time of methylene blue on sol–gel Bi_2FeNbO_7 photocatalysts annealed at different temperatures.

analysis. The small amount of unreacted Fe_2O_3 could play the role of doping in a similar way to that observed in Fe_2O_3/TiO_2 photocatalysts [21]. In this case we would be in the presence of a mixed semiconductor improving the catalytic efficiency.

Since the sol–gel sample of Bi_2FeNbO_7 heated at 400 °C showed the higher photocatalytic activity, we decided to perform a series of tests using the sol–gel samples annealed at 600 and 800 °C. Since at 800 °C the specific surface area is low, we can compare the activity of the Bi_2FeNbO_7 sol–gel catalyst with the solid state materials under the same experimental conditions.

In Fig. 10, the evolution of methylene blue photodegradation as a function of time is shown for the Bi_2FeNbO_7 catalysts obtained by sol–gel (400, 600 and 800 °C) and compared with the solid state catalysts prepared at 1000 °C, the TiO_2 Degussa P-25 reference catalyst is also included.

From the results plotted in Fig. 11, $t_{1/2}$ was calculated and the results are reported in Table 2. The higher activity is showed by Bi_2FeNbO_7 sol–gel catalyst annealed at 400 °C ($t_{1/2}$ = 13 min), which is far of that obtained with the samples calcined at 600 or 800 °C ($t_{1/2}$ = 32 and 47 min, respectively) or to that showed by the solid state material ($t_{1/2}$ = 38 min). Note that these half time

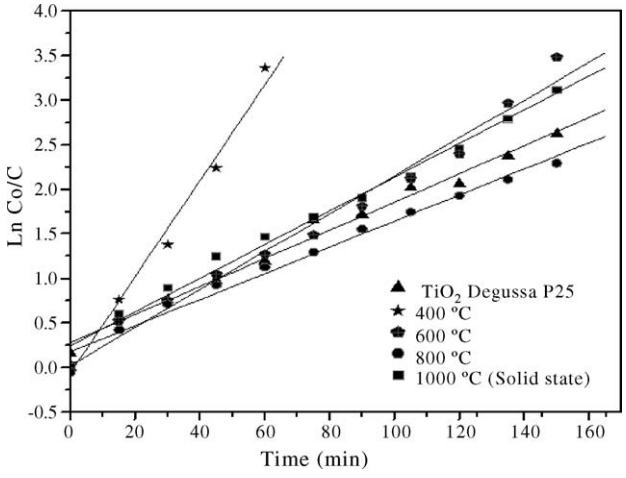

Fig. 11. Plots for kinetic parameters determination on methylene blue degradation on sol–gel Bi_2FeNbO_7 photocatalysts annealed at different temperatures.

life values are lower or similar to that obtained with the TiO_2 Degussa P-25 ($t_{1/2}$ = 45 min) catalyst.

The lower activity showed by the Bi_2FeNbO_7 samples treated at 600 and 800 °C in comparison with the sample calcined at 400 °C can be related to the important decrease in the specific surface area showed by the samples annealed at high temperature. However, the intrinsic semi-conductor properties of low specific surface area composites are maintained.

For comparative study the E_g and kinetic parameters ($t_{1/2}$) for Bi_2MNbO_7 (M = Al^{3+}, In^{3+}, Fe^{3+}, Sm^{3+}) corresponding to ceramic compounds synthesized by solid state method are reported in Table 3. A photoactivity of the same order of that obtained with the Bi_2FeNbO_7 sol–gel sample annealed at 800 °C and to that observed for TiO_2 P-25 catalyst is observed. In spite of their low specific surface area, the Bi_2MNbO_7 ceramic compounds showed photoactivity comparable to TiO_2 catalyst.

4. Conclusions

An alternative sol–gel route for the preparation of Bi_2MNbO_7 (M = Al^{3+}, In^{3+}, Fe^{3+}, Sm^{3+}) is reported. It has been demonstrated that the family of Bi_2MNbO_7 compounds shows an important photocatalytic activity. The Bi_2FeNbO_7 sol–gel (400 °C) catalyst presents the highest photocatalytic activity for the methylene blue degradation. It is highlighted that sol–gel products annealed at 400 °C showed better performance than those prepared by solid state reaction or TiO_2 P-25.

Low specific surface area solid state preparations and sol–gel Bi_2MNbO_7 materials annealed at 800 °C show nearly the same photoactivity, comparable to TiO_2 P-25 reference photocatalyst in the dye photodegradation. A good agreement between E_g and photocatalytic activity was reported.

Acknowledgements

Authors thank CONACYT (Grant 35415-U), SEP-CONACYT (Grant 42910-R) and SEMARNAT (Grant 2004-01-C01-00394) for financial support.

References

[1] M. Schiavello (Ed.), Photoscience and Photoengineering, vol. 3, Wiley, Chichester, 1997.
[2] D.F. Ollis, H. Al-Ekabi (Eds.), Photocatalytic Purification of Water and Air, Elsevier, Amsterdam, The Netherlands, 1993.
[3] N. Serpone, R.F. Khairutdinov, in: P.V. Kamat, D. Meisel (Eds.), Semiconductor Nanoclusters, Stud. Surf. Sci. Catal. 103 (1996) 417.
[4] M.A. Brown, S.C. De Vito, Crit. Rev. Environ. Sci. Technol. 23 (1993) 249.
[5] H. Lacheb, E. Puzenat, A. Houas, M. Ksibi, E. Elaloui, Ch. Guillard, J.M. Hermann, Appl. Catal. B: Environ 39 (2002) 75.
[6] A. Scalfani, L. Palmisano, E. Eavi, J. Photochem. Photobiol. A: Chem. 56 (1991) 113.
[7] O. Legrini, E. Oliveros, A.M. Braun, Chem. Rev. 93 (2) (1993) 671.
[8] K. Sayama, K. Yase, H. Arakawa, K. Asakura, K. Tanaka, K. Domen, T.J. Onishi, Photochem. Photobiol. A: Chem. 114 (1998) 125.
[9] T. Takata, A. Tanaka, M. Hara, J. Kodo, K. Domen, Catal. Today 44 (1998) 17.
[10] N. Kakuta, N. Gota, H. Ohkita, T.J. Mizushima, Phys. Chem. B 103 (1999) 5917.

[11] Z. Zou, J. Ye, H. Arakawa, J. Phys. Chem. 106 (3) (2002) 517.
[12] Z. Zou, J. Ye, H. Arakawa, Mater. Sci. Eng. B 79 (1) (2001) 83.
[13] Z. Zou, J. Ye, H. Arakawa, J. Mol. Catal. A: Chem. 168 (1/2) (2001) 289.
[14] A. Scalfani, L. Palmisano, M. Schiavello, J. Phys. Chem. 94 (1990) 829.
[15] Y. Ikeda, M. Tacana, Y. Bando, Bull. Inst. Chem. Res. Kioto Univ.: JCPDS card 39-0238 64 (1986) 249.
[16] W. Roth, J. Res. Natl. Bur. Stand., Sect. A, JCPDS card 16-0293 66 (1962) 451.
[17] Z. Zou, J. Ye, H. Arakawa, Chem. Mater. 13 (2001) 1765.
[18] T. López Sánchez, P. Bosch, Y. Meas, R. Gómez, Mater. Chem. Phys. 32 (1992) 141.
[19] D. Lide, Handbook of Chemistry and Physics, 71st ed., CRC Press, 1990–1991.
[20] R. Morrison, R. Boyd, Organic Chemistry, 5th ed., Addison-Wesley Iberoamericain, 1990, p. 566.
[21] J.A. Navío, J.J. Testa, P. Djedjeian, J.R. Padrón, D. Rodríguez, M.I. Litter, Appl. Catal. A: Gen. 178 (1999) 191.